Calcium Domains around Single and Clustered IP_3 Receptors and Their Modulation by Buffers

S. Rüdiger,[†] Ch. Nagaiah,[‡] G. Warnecke,[§] and J. W. Shuai[¶*]
[†]Institute of Physics, Humboldt-Universität zu Berlin, Berlin, Germany; [‡]Institute of Mathematics and Scientific Computing, University of Graz, Graz, Austria; [§]Institute for Analysis and Numerics, Otto-von-Guericke University, Magdeburg, Germany; and [¶]Department of Physics, and Institute of Theoretical Physics and Astrophysics, Xiamen University, China

ABSTRACT We study Ca^{2+} release through single and clustered IP_3 receptor channels on the ER membrane under presence of buffer proteins. Our computational scheme couples reaction-diffusion equations and a Markovian channel model and allows our investigating the effects of buffer proteins on local calcium concentrations and channel gating. We find transient and stationary elevations of calcium concentrations around active channels and show how they determine release amplitude. Transient calcium domains occur after closing of isolated channels and constitute an important part of the channel's feedback. They cause repeated openings (bursts) and mediate increased release due to Ca^{2+} buffering by immobile proteins. Stationary domains occur during prolonged activity of clustered channels, where the spatial proximity of IP_3Rs produces a distinct $[Ca^{2+}]$ scale (0.5–10 μM), which is smaller than channel pore concentrations (>100 μM) but larger than transient levels. While immobile buffer affects transient levels only, mobile buffers in general reduce both transient and stationary domains, giving rise to Ca^{2+} evacuation and biphasic modulation of release amplitude. Our findings explain recent experiments in oocytes and provide a general framework for the understanding of calcium signals.

INTRODUCTION

The modulation of cytosolic calcium concentrations is a fundamental part of many cell-signaling networks. The calcium-rich endoplasmic reticulum (ER) releases Ca^{2+} through inositol 1,4,5-trisphosphate receptor channels (IP_3 R) present in the ER membrane into the cytosol where concentrations of Ca^{2+} are normally low (1). IP_3 Rs regulate Ca^{2+} release in response to binding of Ca^{2+} and IP_3 to receptor sites on the cytosolic side of the channels (2). Rebinding of liberated calcium to channels increases the open probability and provides a self-amplifying mechanism called calcium-induced calcium release. Ca^{2+} released from a channel diffuses in the cytosol and increases the open probability of neighboring channels by binding to activating binding sites. Subsequently, increased Ca^{2+} concentrations lead to closing of channels by binding of Ca^{2+} to inhibiting sites.

An important aspect of coupling by diffusing Ca^{2+} is the existence of multiple spatial scales and a related hierarchy of coupling strengths. At one end of the spatial spectrum are short openings of single channels called blips, where, in a self-loop, released Ca^{2+} causes small close times and bursts of openings. Experimental observation of larger but still localized release events called puffs (3,4) indicates that functioning IP_3 R channels are grouped into clusters on the ER membrane containing, at most, a few tens of channels. The small number of channels and their proximity lead to stochastic but cooperative openings concerted by local diffusion of Ca^{2+} and calcium-induced calcium release between adjacent channels (5,6). It has been argued that the different coupling strength between channels within the same cluster and those in different clusters is responsible for the hierarchical occurrence of puffs and cell-global release (7–9). According to this picture, global release occurs from clusters across the ER membrane at spacings of a few micrometers and requires synchronization of many clusters to form global oscillations and waves (4,10–12).

The complex role of calcium binding proteins (buffers) is a key issue in the modeling and understanding of diffusive coupling of IP_3 Rs. By binding and unbinding of calcium, buffers modify the equilibrium concentrations and are thus useful to experimentally change rest level concentrations of free calcium. However, the spatial and dynamical properties of coupled calcium/buffer systems are not well understood. Experiments with various exogenous buffers demonstrate the strong effect on the release that buffers can have (7,13,14). Dargan et al. (7,14) studied how the response of the Ca^{2+} signal depends on the binding kinetics of Ca^{2+} and buffers. The reaction to a stepwise increase of IP_3 was either a shortened release spike (for slow-binding buffer) or a prolonged release tail (for fast buffer).

The same authors also suggested that different buffers disrupt Ca^{2+} feedback on different spatial scales. The influences of buffer can be distinguished following the hierarchy of the calcium system (i.e., influence on coupling between clusters, channels inside of a cluster, and self-feedback of a channel). In a modeling approach, Zeller et al. (8) and Falcke (15) studied the release from an array of clusters under the presence of buffers. On the other hand, the buffer effects on Ca^{2+} released from a single deterministic channel were numerically and analytically discussed in the literature (16–19). Swillens et al. (5) investigated a stochastic IP_3 R

Submitted August 31, 2009, and accepted for publication February 26, 2010.

*Correspondence: jianweishuai@xmu.edu.cn

Editor: Arthur Sherman.

0006-3495/10/07/0003/10 $2.00

doi: 10.1016/j.bpj.2010.02.059

model within a cytosol-like environment and discussed the effect of various dye buffers on blip dynamics. A single channel in an immobile-buffer environment was studied numerically by Shuai et al. (20). The authors simulated the release dynamics of IP_3 Rs based on a stochastic nine-state model fitted to recent patch-clamp data (21). They found that reactivation of the channel depends strongly on immobile (or stationary) cytosolic Ca^{2+} buffers. Immobile buffer delays the collapse of local Ca^{2+} microdomains after each closure, when concentrations drop from >100 μM to rest levels of <0.1 μM.

We now extend this work by studying different buffers and combinations of buffers as well as by studying their effect on interaction of channels within a cluster. In this way, we close the gap between the available research on arrays of clusters and single channels. We identify the collapse of calcium domains as one of two important stages of intervention by buffers. While the transient lingering of free calcium ions after closing of channels dominates behavior of single channels, we find that release from clusters is determined by sustained calcium levels in the cluster area. A nontransient domain is maintained by repeated openings of channels in the cluster and can thus be regarded as a stationary (although fluctuating) attribute of release.

Mathematically, stationary domain calcium concentration is defined as a suitable average over time and over the individual channel domains in a cluster. We numerically determine its dependence on cluster geometry and buffers. In contrast to earlier work (8) we employ a three-dimensional, fully spatially resolved model of a cluster, that is, individual channels are located on the membrane with a certain separation from each other. This method allows us to show, for instance, that the level of stationary calcium falls with mobile buffer due to evacuation of calcium between channels and three-dimensional transport away from the cluster. Based on these results, we suggest that further analytical approaches should be built on cluster models with spatially separated channels rather than with one continuous source area (6,22,23).

HYBRID STOCHASTIC AND DETERMINISTIC MODEL FOR CALCIUM DYNAMICS AND NUMERICAL METHODS

The model consists of partial differential equations for concentration fields and a Markovian description of discrete stochastic quantities. The concentration fields are the calcium concentration in the cytosol and the concentration of one or two buffers bound to calcium. Stochastic quantities are the discrete states of channel subunits, which determine the open/close states of each channel. We here adopt the nine-state model for the gating of subunits (21,24). Compared to the standard DeYoung-Keizer model (25) the nine-state model possesses an additional active state, which represents a conformational change of the subunit related to the channel opening (see Stochastic Model of Channel Gating in the Supporting Material).

The calcium concentration in the cytosol is determined by diffusion, the transport of calcium through the ER membrane, and the binding and unbinding of calcium to buffer molecules. In the cytosol, we consider the following types of buffers: exogenous mobile buffer with fast or slow reaction kinetics and a stationary buffer. Buffers are assumed to be distributed homogeneously at initial time. Parameters for the mobile and stationary types of buffers used for this work are listed in Table S1 in the Supporting Material.

The equations are either solved in a spherically symmetric domain (single channel) or in a cubelike domain. For the setup with a single IP_3 R channel that is located in the center of the cytosolic space, we use spherical symmetry to simplify the reaction-diffusion part of the model to a one-dimensional problem (20). The finite difference method proposed by Smith et al. (18) was used to solve the ensuing partial differential equations.

For release from several channels, the symmetric reduction is not possible. Instead, we use a cuboid of 5-μm height, where the bottom surface represents an idealized ER membrane of 8-μm side length (see Fig. 2 *A*). The bulk of the cube represents the cytosol of the cell, while boundary conditions at the bottom surface account for the membrane current consisting of channel, pump, and leak contributions. Channels are placed with a certain spatial separation d on the surface. This method is distinct from the two-dimensional simulations in Zeller et al. (8), where all channels of a cluster were placed in a common source area. Our numerical method consists of coupled solvers for the deterministic set of partial differential equations and the stochastic equations. In view of the multiple space- and timescales, we employ a conforming finite element method for the spatial discretization and an adaptive linear implicit time-stepping for the deterministic part (26). The stochastic channel gating is incorporated by using the recently devised hybrid method (27). In (27) we established the equivalence of cuboid and spherical simulation results for single channels, which allowed us to use the reduced one-dimensional diffusion model with Markovian channel dynamics to save computation time for our current work. For a more detailed description of model equations and numerical methods, see section S1 and S2 of the Supporting Material.

RESULTS FOR SINGLE CHANNEL DYNAMICS

For an isolated channel, we will first discuss the case of a single buffer, either immobile or mobile and then extend the discussion to the case of two buffers acting simultaneously. Shuai et al. (20) studied the dynamics of a single channel in the presence of stationary buffer and found a strongly shortened mean close time with almost unchanged mean open time, and thus an overall increase of open

probability at large buffer concentrations (*squares* in Fig. 1, *A–C*). This effect results from the fact that stationary buffer extends the lifetime of Ca^{2+} domains around active channels beyond the time when the channel has already closed (*dotted line* in Fig. 1 *E*). The buffer-bound Ca^{2+} will be released relatively slowly after the channel has closed and may subsequently bind to the channel and open it again, leading to bursts of channel openings and closings.

Mobile buffer alone has little effect on single channel dynamics

We next consider mobile buffers either with slow reaction kinetics (representing EGTA) or fast reaction kinetics (BAPTA). The results are included in Fig. 1, *A–C* (*up-triangles* for BAPTA and *down-triangles* for EGTA). In contrast to the case of immobile buffer, increasing mobile buffer concentration has little effect on the single channel dynamics.

To elucidate the different action of mobile and immobile buffer on channel closing, we made deterministic simulations with a channel opening for 6 ms, which is the mean open time of a single channel (Fig. 1 *B*). Fig. 1, *D* and *E*, shows the local Ca^{2+} concentration at the channel pore during and after channel openings with different concentrations of BAPTA and EGTA. Fig. 1, *D* and *E*, demonstrates that the decay rate of the free Ca^{2+} concentration at the channel pore increases as a function of increasing concentration of mobile buffer. This occurs because mobile buffers bind the released free Ca^{2+} ions at the channel pore and act as a shuttle to carry the Ca^{2+} ions away from the channel pore. BAPTA is a faster binding/unbinding buffer than EGTA, thus a larger decay rate can be observed for BAPTA than EGTA at the same buffer concentration. The fast decay of $[Ca^{2+}]$ after channel closing explains the ineffectiveness of mobile buffer in reopening of channels. For comparison, the local Ca^{2+} concentration at the channel pore with the 800 μM immobile buffer is also plotted in Fig. 1 *E*, showing the opposing effect on Ca^{2+} decay after channel closing discussed above.

In Fig. 1, *A–C*, blip dynamics are characterized for IP_3 concentrations at 0.2 and 1.0 μM. Generally, a larger open probability with a smaller close time is obtained with increased IP_3 concentration.

Mobile buffer competes with stationary buffer and reduces opening probability in two-buffer setups

Now we discuss the effects of EGTA and BAPTA on single channel dynamics in the presence of stationary buffer. The immobile buffer is fixed at 800 μM in the system. With increasing mobile buffer concentration, the mean close time increases strongly (data shown in Fig. S1 *A*) with a slightly increased mean open time (Fig. S1 *B*), resulting in a decrease of the open fraction (Fig. S1 *C*). The 800-μM

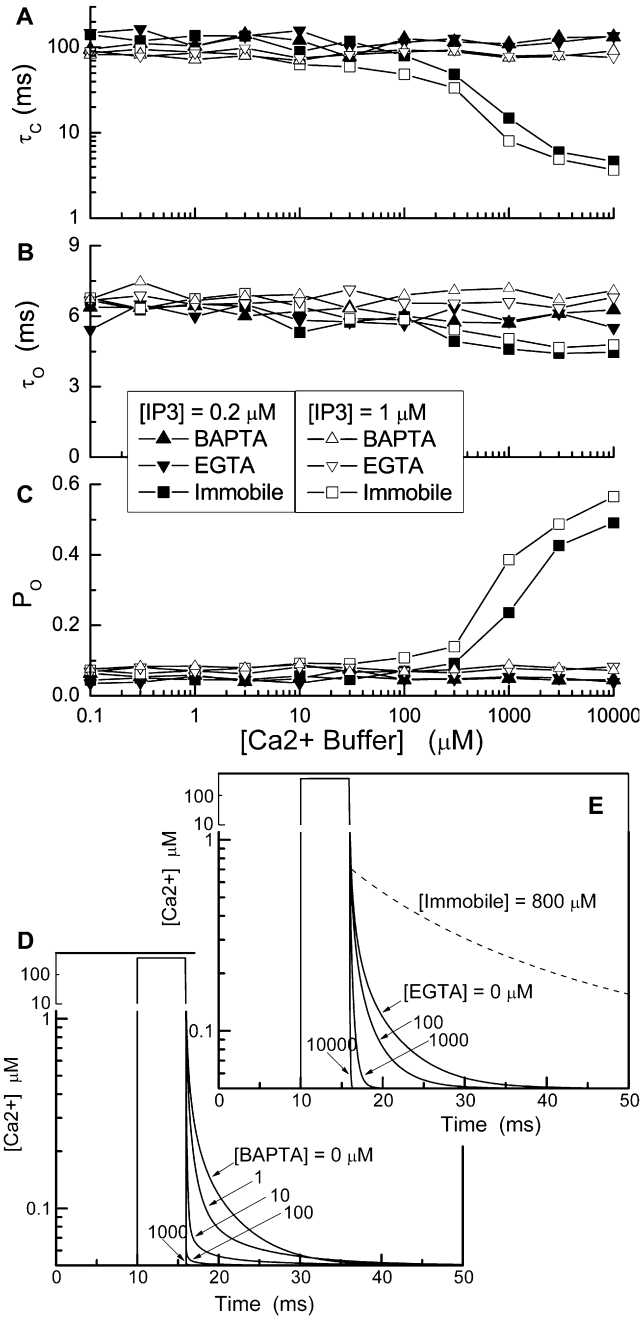

FIGURE 1 The blip dynamics as a function of the concentration of an immobile buffer or a mobile buffer for IP_3 concentrations of 0.2 and 1.0 μM. (*A*) Mean close time. (*B*) Mean open time. (*C*) Open probability. The effects of mobile buffers on the decay rate of the free Ca^{2+} concentration at the channel pore are shown in panels *D* and *E*. The Ca^{2+} concentration at the channel pore is plotted as a function of time with the channel held open for 6 ms. (*D*) BAPTA at concentrations of 0, 1, 10, 100, and 1000 μM and (*E*) with EGTA at concentrations of 0, 100, 1000, and 10,000 μM. The dashed line shows the evolution under the presence of immobile buffer.

immobile buffer will cause a slow decay of Ca^{2+} concentration after channel closing. However, mobile buffer acts as a shuttle to carry the Ca^{2+} ions away from the channel pore. The free Ca^{2+} concentration will diminish to its

resting-state level within a shorter time, resulting in a smaller chance for the channel to reopen. Thus, the higher concentration of mobile buffer causes a longer mean close time and a smaller open probability.

Fig. S1 also shows that the mean open time of a single channel is insensitive to both EGTA and BAPTA buffers. However, the mean close time and the open probability show different behaviors for the two types of mobile buffers in the range of 1–1000 μM. From Fig. 1, *D* and *E*, it can be seen that the shuttle effect on free calcium after channel closing for 10-μM BAPTA is similar to that for 1000-μM EGTA. Thus, the open probability of the channel with 3-μM BAPTA is similar to that with 1000-μM EGTA (Fig. S1 *C*). The differences for both the mean close time and the open probability become less significant for EGTA and BAPTA buffers at large concentrations. The shuttle effect for mobile buffer at large concentration is so strong that the slow decay caused by the immobile buffer will no longer exist, no matter if the mobile buffer is fast or slow. The IP_3 R dynamics in this case reaches the limiting situation of absence of buffers. Indeed, the open probability of ~0.05 with mean open time close to 6 ms and mean close time close to 100 ms is similar to the result given in Fig. 1. Our results have been summarized qualitatively in columns 2 and 3 of Table 1.

We have also studied the effects of changing the diffusion coefficient and the IP_3 concentration on single channel dynamics. A discussion is included in Single-Channel Simulations in the Supporting Material and in Fig. S2 and Fig. S3.

MULTICHANNEL SIMULATIONS

To test the significance of our single-channel results, we simulated the release dynamics of a cluster with nine channels using the hybrid simulation method. Channels were arranged in a 3×3 grid with grid distances d from 15 to 1000 nm (Fig. 2 *A*). Generally, we simulated for a total of 11 s and recorded the number of open and inhibited channels as well as the calcium and buffer distributions at the membrane. In the simulations presented below, the channels were stimulated by a step increase of [IP3] from 0.01 to 0.2 μM at time $t = 1.0$ s, unless stated otherwise. Channels opened stochastically and cooperatively so that the random opening of a first channel normally triggered opening of further channels. Fig. 2 *B* shows a representative evolution of the free Ca^{2+} concentration at the pores of three selected channels for $d = 30$ nm (no buffer). An open channel can be identified by a Ca^{2+} concentration at the pore, $[Ca^{2+}]_{pore}$, that exceeds 100 μM. On the other hand, if a channel is closed, but one or more other channels are open, $[Ca^{2+}]_{pore}$ falls to ~10 μM, even if a channel is closed very briefly. If all channels are closed sufficiently long, $[Ca^{2+}]_{pore}$ decreases to the rest level of 0.05 μM.

As before in the case of a single channel, the level of Ca^{2+} concentration at the mouth of a closed channel determines the probability to open again and thus to undergo bursts of repeated openings and closings. Because of its role as a mediator of buffer effects on channel gating, we will refer to the suitably averaged, local concentration of Ca^{2+} as cluster domain concentration. We will first discuss the case of immobile buffer and mobile buffer separately, and then study the case of two combined buffers.

TABLE 1 Qualitative dependence of calcium concentrations and open probabilities on three types of buffer

Buffer	Isolated channel		Clustered channels	
	Transient $[Ca^{2+}]$	P_o	Stationary $[Ca^{2+}]$	P_o
Immobile	↑ ↑	↑	→	→
Fast	↓ ↓	↓*	↓	↑† ↓
Slow	↓	↓*	→	→

Up/down arrows indicate whether a quantity increases or decreases, respectively.

*Here we assumed an environment of immobile buffer, where addition of mobile buffer eliminates transient domains and decreases open probabilities.

†The increase of open probability only occurs under certain conditions. For instance, for very closely packed clusters without additional buffer, we found strong inhibition. An increase of fast buffer concentration then decreases $[Ca^{2+}]_{dom}$ below the dissociation constant of inhibition. As a result, a reduction of inhibition occurs and thus the open probability can increase (see Fig. 5 *A*). For larger channel distances, domain Ca^{2+} values may already be below K_{inh} before addition of buffer and the dominant effect is a decrease in activation (compare Fig. 6).

Open probability is independent of stationary buffer for clusters of channels

We calculated mean quantities as averages for the time interval from 1 s to 11 s using output time steps of 1 ms, to characterize the long time gating behavior. We found above that for a single channel the open probability is close to 5% if no buffer is present. The open probability strongly increases with increasing amounts of stationary buffer (see Fig. 1). Surprisingly, for the nine-channel setup, no clear dependence of the open probability on immobile buffer concentration was found for channel distances of up to 120 nm (Fig. 3). Linear fits show that P_o is approximately constant, for instance at ~0.2 for $d = 30$ nm. P_o increases with d, reaches a maximum of ~0.3 at intermediate channel distances of 120 nm, and decreases again for larger channel distances.

In contrast to small and intermediate d, for channel distances of 1000 nm, the open probability increases with the buffer concentration (Fig. 3) for $[B_{imm}] > 80$ μM. We note that for large distances, the coupling of channels is small, so that one recovers the case of individual channels in which the open probability increases strongly with the buffer concentration.

To elucidate the different behavior of single and clustered channels we will now discuss the concentration of free Ca^{2+} in the cluster area and its modulation by buffer. Because only the free calcium concentration at the binding site, $[Ca^{2+}]_{pore}$, enters the gating behavior of a channel, we evaluated the calcium concentrations at each of the nine channel's pores. The distribution of channel pore concentrations at all times and all channels is shown in Fig. 4 (for all distribution,

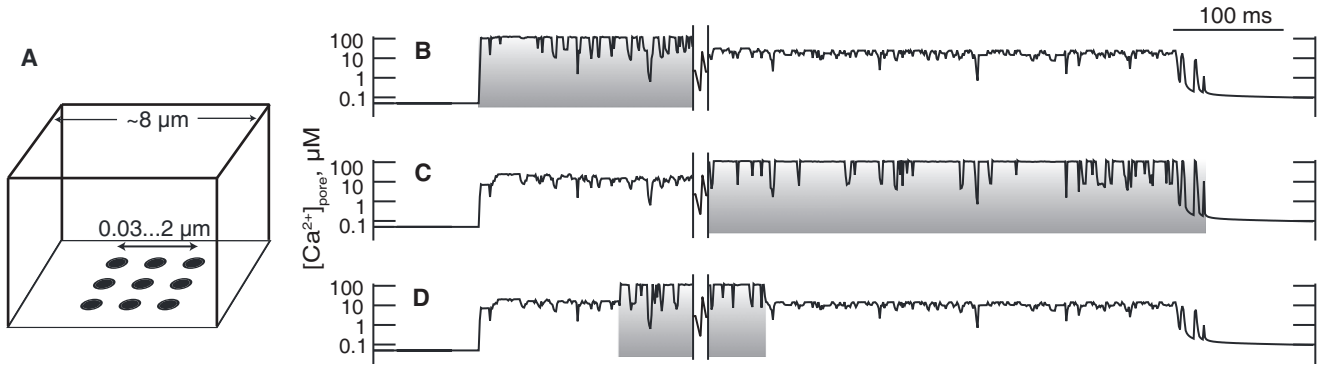

FIGURE 2 (*A*) Schematic plot of the computational model for a cluster of nine channels. The lower surface represents the ER membrane. (*B–D*) Evolution of free calcium concentration at the channel center for three representative channels. In this simulation, $d = 30$ nm, and no buffer was used. Release bursts are indicated by the underlaid shaded boxes. If a channel is open, the Ca^{2+} concentration reaches >100 μM. However, if a channel is closed but other channels in the cluster are open, the concentration falls to ~10 μM within <1 ms, approximately independent on the distance from an active channel.

we excluded instances of $[Ca^{2+}]_{pore} < 0.051$ μM). The plots represent the overall distribution (Fig. 4 *A*), the distribution for times when all channels are closed (Fig. 4 *B*), and the distribution of values at closed channels in the presence of open channels (Fig. 4 *C*). In the overall distribution (Fig. 4 *A*) for control (no buffer), three qualitatively different contributions were found. At ~100 μM we identify the local concentration at open state (peak 1). A second contribution occurs between 0.05 and 0.1 μM (peak 2). As can be concluded from comparison with Fig. 4 *B*, this maximum corresponds to a transient calcium concentration, which relaxes to rest level after all channels have closed. A third contribution at ~10 μM (peak 3) represents channels that are closed, but where different channels in the cluster are open (compare Fig. 4 *C*).

Now we turn to the case of immobile buffer. The largest difference to the prior case occurs in plot Fig. 4 *B*, which shows the distributions of $[Ca^{2+}]_{pore}$ at times when all channels have closed. For immobile buffer, a much higher presence of calcium was found. This results from the effect of immobile buffer, as discussed in Results for Single Channel Dynamics—namely that it delays the relaxation to rest state and thus, strongly increases the transient calcium. As the open probability in clusters is insensitive to immobile buffers, it follows that P_o cannot depend on the amplitude of transient domains. On the other hand, the distribution in Fig. 4 *C*, which corresponds to a sustained (or stationary) calcium elevation, is not changed significantly compared to the control case. Therefore, P_o may still be changed if the amplitude of stationary domains is modulated (see below). We tentatively conclude from this consideration that the distributions shown in Fig. 4 *C*, but not those in Fig. 4 *B*, determine the release amplitude in clusters.

Adjacent active channels determine local Ca^{2+} concentration at closed channels

The persistence of the calcium distribution shown in Fig. 4 *C* and its narrow base under addition of immobile buffer suggests that we further consider the average concentration of this distribution. We will show that this average calcium value is strongly related to the changes of open probability for varying channel distance d and concentration of fast mobile buffer. The average thus characterizes the relevant calcium concentration of the cluster.

If $c_i(t)$ is the Ca^{2+} concentration at the mouth of channel i, ($i = 1,\ldots, N = 9$) at time t (t from $t_0 = 1,\ldots t_1 = 11s$) and $o_i(t)$ is the open or close state of the channel (i.e., $o_i = 0$, closed, or 1, open), we define

$$\left[Ca^{2+}\right]_{dom} = \sum_i \frac{1}{NT_i} \int_{t_0}^{t_1} c_i(t)(1 - o_i(t))\ \mathrm{sgn}(N_o(t))dt, \quad (1)$$

where

$$T_i = \int_{t_0}^{t_1} (1 - o_i(t))\ \mathrm{sgn}(N_o(t))dt$$

is the total time that the i^{th} channel is closed but at least one other channel is open, where

$$N_o(t) = \sum_i o_i(t)$$

is the number of open channels at time t and sgn(x) gives +1 if x is positive and 0 if $x = 0$. The cluster domain concentration $[Ca^{2+}]_{dom}$ is the average concentration that a channel is subjected to if it is closed but the cluster is active.

$[Ca^{2+}]_{dom}$ for different channel distances and different $[B_{imm}]$ is shown in Fig. 3 *B*. First, we argue that the $[Ca^{2+}]_{dom}$ value is constant with increasing amounts of immobile buffer. In contrast, the average, that is taken after closing of all channels, increases as it does in the single-channel case (data not shown). Furthermore, we found that $[Ca^{2+}]_{dom}$ values decrease with the channel distance. It is ~10 μM at 30 nm, 5 μM for 120 nm, and as small as 0.5 μM at 1000 nm. Fig. 3, *A* and *B*, indicates that the domain

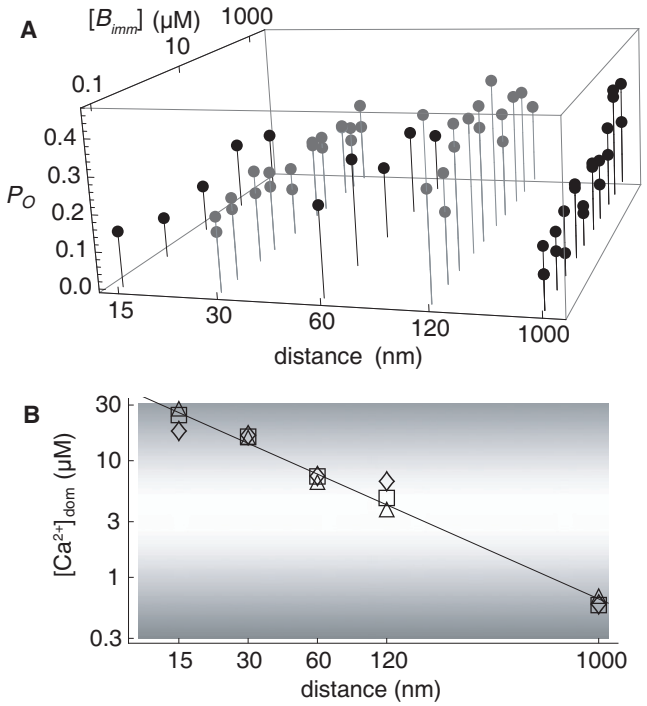

FIGURE 3 (*A*) The mean open fraction depends on the distance d between channels but it does not depend on the amount of immobile buffer (except for large channel distance $d = 1000$ nm). For each pair of parameters (d,[B_{imm}]), one or two simulations of 10 s were evaluated and results are represented by circles attached to the pins. (*B*) The stationary concentration $[Ca^{2+}]_{dom}$ does not vary with [B_{imm}] (◇, 0.08 μM, □, 80 μM, and △, 8000 μM), but strongly decreases with channel distance d. The reduction of $[Ca^{2+}]_{dom}$ with cluster size results in larger probability of a subunit to be in the active state X_{ACT} (*open horizontal area*) for intermediate distances at ~120 nm and small probability for very small and very large distances (*dark shaded areas*). The shading scale has been obtained from Eq. 2 with $K_{act} = 0.8$ μM and $K_{inh} = 16$ μM. (*Solid line*) Fitted calcium domain as a function of distance. The cross-point of the solid line with the central open area is at ~200 nm.

calcium concentration determines the open probability. It remains to us to consider why P_o exhibits a maximum at intermediate channel distances. We first note that domain calcium values for intermediate d are close to the dissociation constants of inhibition ($d_2 = 16$ μM) and activation ($d_5 = 0.8$ μM). We therefore suggest that the open probability should be largest if the domain calcium concentration $[Ca^{2+}]_{dom}$ is ~2–5 μM (large activation and small inhibition). To make this observation more precise, we can estimate the probability of a subunit to be activated and not inhibited (i.e., the subunit is in the state X_{ACT}) as the product of three factors

$$P_{s.u.} = \frac{a_0}{a_0 + b_0} \frac{[Ca^{2+}]_{dom}}{K_{act} + [Ca^{2+}]_{dom}} \left(1 - \frac{[Ca^{2+}]_{dom}}{K_{inh} + [Ca^{2+}]_{dom}}\right). \quad (2)$$

The second and third factors determine the probability for a subunit to be active and not inhibited, respectively, while the first factor calculates the fraction of time spent in the active state compared to the state X_{110} (a_0 and b_0 are the on- and off-rates of the transition from X_{110} to the active state). $K_{act,\ inh}$ values are dissociation constants of activating and inhibiting binding processes. $P_{s.u.}([Ca^{2+}]_{dom})$ has been gray-shaded in Fig. 3 *B* under the assumption of large IP_3 concentration, showing that largest activation probabilities occur for ~200-nm channel distance, which is the cross-point of the open white area and the solid line of the linearly fitted domain calcium as a function of distance. This observation is consistent with the larger open probability for the channel geometry of 120 nm distance compared to 30 nm and 1000 nm smaller and larger distances.

Mobile buffer affects Ca^{2+} release in two regimes

A strong impact of buffer was found for the case of mobile buffer with fast reaction kinetics (corresponding to BAPTA). The open probability for a setup with 30-nm channel distance is shown in Fig. 5 *A*. For small buffer concentration,

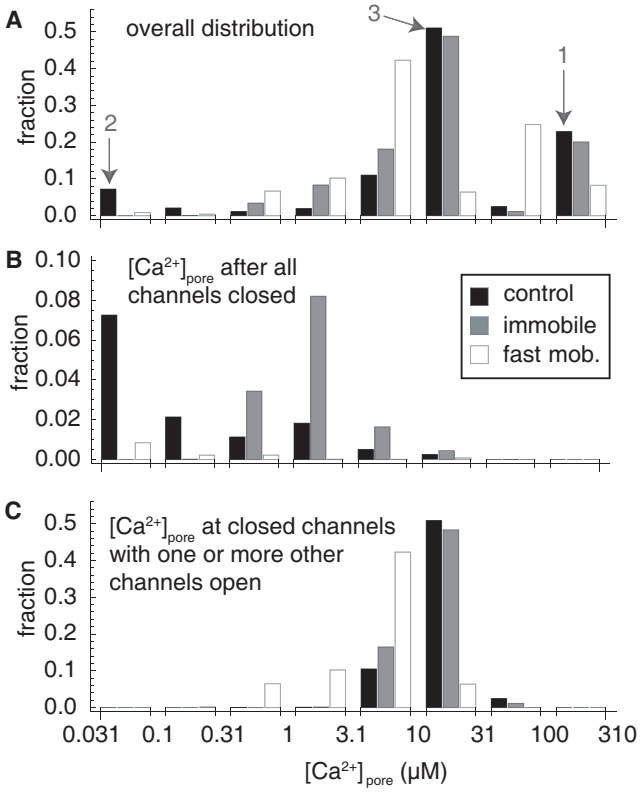

FIGURE 4 Distribution of channel mouth Ca^{2+} concentrations for runs without and with two different buffers. The three plots show the overall distributions (*A*), the distributions of Ca^{2+} concentrations when all channels are closed (*B*), and the distributions of Ca^{2+} concentration at a channel when it is closed, but other channels in the cluster are open (*C*). Each bar corresponds to one simulation over 10 s for control, 800 μM stationary buffer, or 800 μM fast mobile buffer. We have neglected instances where $[Ca^{2+}]_{pore} < 0.051$ μM. Numbers at arrows denote the order by which peaks are mentioned in the main text.

the open probability is close to the value of 0.2, which was found before for the case of stationary buffer or without buffer. However, with increasing buffer concentration the open probability increases to levels >0.3 at 2000 μM concentration. If the buffer concentration is further increased, the open probability decreases strongly to 0.1. In effect, there is a distinct maximum of the open probability for buffer concentrations at ~2000 μM. For EGTA (slow mobile buffer), no significant effect was found.

To elucidate the behavior for BAPTA, we have plotted the cluster domain concentration $[Ca^{2+}]_{dom}$ and the fraction of inhibited channels in Fig. 5 *B*. For increasing amounts of BAPTA, $[Ca^{2+}]_{dom}$ decreases from ~16 μM to 0.1 μM. This effect can also be seen from Fig. 4 *C*, where for fast mobile buffer the distribution moves to the left compared to the other two cases. Accordingly, only for small amounts of mobile buffer are many channels inhibited. For larger buffer concentration, $[Ca^{2+}]_{dom}$ and inhibition are reduced resulting in a large P_o. For amounts of buffer beyond 4 mM, $[Ca^{2+}]_{dom}$ is becoming even smaller and loses its capacity to stimulate frequent openings of neighboring channels. This corresponds to a strong isolation of channels, so that for large mobile buffer concentration the open probability of individual channels, at ~5%, is recovered.

To quantify this argument we will now make an estimate of the open probability. We first observe that the logarithm of the domain calcium concentration assumes an almost linear behavior if plotted against the buffer concentration in linear scale (Fig. 5 *B*, *inset*). We therefore approximate

$$\left[Ca^{2+}\right]_{dom} = C_0 e^{-\alpha B_m}, \quad (3)$$

where B_m denotes the total amount of mobile buffer, $C_0 = 16$ μM is the estimated domain concentration at $B_m = 0$, and α is a fitting constant obtained (as shown by the *straight line* in Fig. 5 *B*, *inset*).

Using the argument of the previous section, the open probability of a channel is then obtained from the fact that three or four subunits should be in the active state,

$$P_o = P_{s.u.}^4 + 4P_{s.u.}^3(1 - P_{s.u.}), \quad (4)$$

where $P_{s.u.}$ is given by Eqs. 2 and 3. This expression has been evaluated to the solid line in Fig. 5 *A*, clearly showing qualitative agreement with the numerical data points and proving the significance of the domain calcium concentrations for the open probability.

The decrease of domain calcium originates from the narrower microdomains around open channels. This can be clearly seen in Fig. S4 *C*, which shows that $[Ca^{2+}]$ is almost at rest level at the location of closed channels for large B_m. We therefore conclude that addition of fast mobile buffer strongly reduces the coupling of channels within a cluster by diffusing calcium. Note that for large amounts of BAPTA the $[Ca^{2+}]_{dom}$ reduction down to 0.1 μM can be even stronger than the spatial decoupling by placing the channels

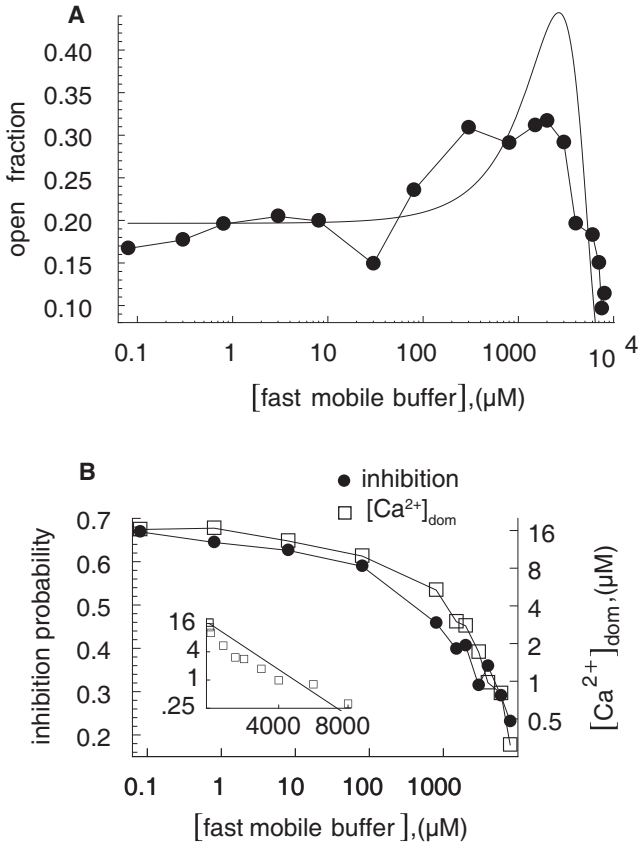

FIGURE 5 Simulations with various amounts of mobile buffer with fast reaction kinetics (BAPTA) and grid constant $d = 30$ nm. (*A*) Open probability (to reduce fluctuations we have averaged over 20 s for each data point). The smooth curve shows the analytical approximation using Eq. 4 and $K_{act} = 0.8$ μM, $K_{inh} = 16$ μM. (*B*) Fraction of inhibited channels and the cluster domain calcium. (*Inset*) Exponential fitting of the cluster domain concentration ($\alpha = 5.64 \times 10^{-4}$ μM^{-1}).

1 μm apart, in which case $[Ca^{2+}]_{dom}$ values are close to 0.5 μM. Our results for mobile buffer have been summarized in columns four and five in Table 1.

Immobile buffer is also ineffective in two-buffer environments of clustered channels

The contradiction between the effects of immobile buffer in mono- and multichannel setups motivated us to also consider the case of two simultaneous buffers for clusters. Specifically, we now discuss cluster simulations for immobile buffer combined with fast mobile buffer. The decrease of $[Ca^{2+}]_{dom}$ for fast mobile buffer that we found can be interpreted as follows: Fast mobile buffer binds released calcium and shuttles it away, thus reducing the size of the calcium domains around each open channel (Fig. S4 *C*). For very large buffer concentration this corresponds in effect to a growing spatial isolation of channels, similar to a very large distance d of channels. Further, for isolated channels we had seen earlier that immobile buffer

has a strong impact on the open probability by delayed release of bound calcium. It is therefore possible that immobile buffer counteracts the effect of fast buffer and increases P_o by a mechanism similar to the one for an isolated channel. We ask now if there is a significant change of P_o for immobile buffer in the presence of large quantities of fast mobile buffer.

The open probability for various mobile buffer concentrations and zero or 8000 μM immobile buffer is shown in Fig. 6 (see Two-Buffer Simulations for Multichannel Setup in the Supporting Material for information on the simulation method based on larger pores). It is apparent that the open probability decreases for large mobile buffer concentrations, but does not depend on the amount of immobile buffer. This result shows that immobile buffer does not modify cluster release amplitude even in the presence of large amounts of mobile buffer. This occurs because, similar to the mechanism for the single-channel with two buffers, mobile buffer rapidly destroys local calcium domains after a channel has closed. Thus, even in the presence of high quantities of immobile buffer, the probability to reopen is not modified.

Fig. 6 also shows the experimental dependence of calcium release amplitude measured by Dargan and Parker (7). They have estimated the maximal fluorescence level V_{max} for saturating levels of IP_3 and various amounts of BAPTA buffer (*solid diamonds*). V_{max}, which is an indirect measure of calcium release, increases slightly for small levels of BAPTA (compared to the control case), but decreases sharply for values of 100 μM and above. While the relatively low spatial resolution of experimental measurements does not allow the estimation of release amplitudes of individual channels or clusters, we here suggest that the lower overall amplitude is due to the decrease of open channel numbers for each cluster. In that respect, the good agreement with our simulation results shows that the intervention of BAPTA between the channels of a single cluster discussed in this article is sufficient to explain the experimentally observed decrease of global calcium release. This finding demonstrates the significance of our analysis for whole-cell release properties.

In contrast to the simulations for a channel distance of 120 nm, the 30-nm case exhibits a decrease in calcium release at much higher values (compare Fig. 5). This comparison suggests that the actual channel distance in clusters of *Xenopus* oocytes is closer to 120 nm than to 30 nm. It also implies that the cluster typically has a relatively large size, which has been first proposed in Shuai et al. (28) and confirmed experimentally in Demuro and Parker (29).

We finally note that our results are independent of IP_3 concentration. The inset in Fig. 6 shows that for IP_3 concentration increased to 1.0 μM, the reduction of P_o occurs at approximately similar values to BAPTA concentration. This finding supports our interpretation that the effects of buffer on calcium release are mediated directly through the cluster domain calcium concentration.

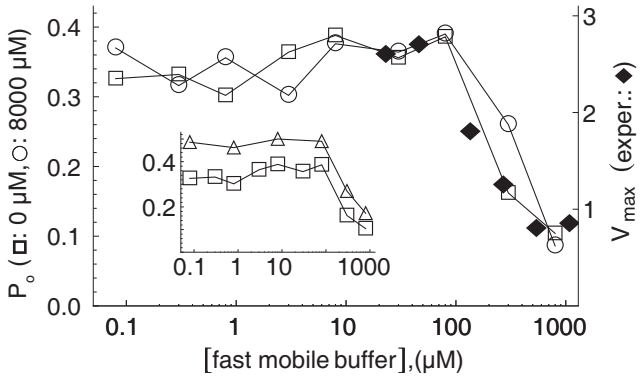

FIGURE 6 The open probability for various amounts of fast mobile and stationary buffer in a setup with nine channels and 120-nm channel distance (*open symbols*). Each data point is an average over 50 s. These results were obtained using the large-pore method under the presence of fast mobile buffer and zero (□) or 8000 μM (○) stationary buffer. For comparison we have plotted the amplitude of Ca^{2+} release obtained in experiments on *Xenopus* oocytes (see Fig. 4 *B* in (7)). (◆) Peak fluorescence level V_{max}. The right axis has been scaled to match the values of simulations and experiments for vanishing amount of mobile buffer. (*Inset*) P_o for two different IP_3 concentrations of 0.2 (□) and 1.0 μM (△).

CONCLUSIONS

Our simulations have shown a strong dependence of calcium release on buffer. For a single channel we found that its open fraction increases and the mean closed time decreases with the concentration of an immobile buffer, whereas mobile buffer alone does not change release dynamics. The increase of open probability with immobile buffer results from the slower decay of $[Ca^{2+}]$ after channel closing, which is not observed for mobile buffer. A different picture emerges if one considers two buffers simultaneously. We found that a sufficiently large amount of mobile buffer counteracts the release-increasing effect of immobile buffer and reduces open probability. Mobile buffer takes up calcium from the stationary buffer after the channel has closed and shuttles it away. Therefore, the delaying effect of immobile buffer is lost. This effect is observed both for fast and slow mobile buffer; however, due to the smaller reaction rate, the effect is much smaller for slow buffer (Table 1, second and third column).

Because of the strong effect of immobile buffer for a single channel it came as a surprise that it is ineffective in clusters of channels. Here we found no influence of immobile buffer on the open probability. The reason is the typically large concentration of calcium in the cluster area as a whole. Because on average ~20% of the channels are open for IP_3 concentrations of 0.2 μM without additional buffer (i.e., there are always approximately two of nine channels open), the released calcium keeps the concentration relatively high at ~10 μM. This concentration is much higher than the typical calcium concentration after closing of an isolated channel (<0.7 μM, see Fig. 1 *E*), and therefore, in a cluster of channels, the transient calcium is of negligible

importance compared to the calcium arriving from neighboring channels.

We also found that, in contrast to the single channel simulations, fast mobile buffer has a strong effect on multichannel dynamics even if used in a one-buffer environment. We therefore obtain a reversal of the findings for a single channel. Note that the inefficiency of immobile buffer in the multichannel case was even found for two simultaneously acting buffers. Based on these results, one can neglect the immobile buffer, at least in the case of sustained release for large IP_3 concentration, when at least one channel stays open.

To further elucidate the contrasting pictures for single and clustered channels we have calculated the average pore concentration for channels at those times, at which they are closed, provided that different channels in the cluster are open. This concentration, which we call cluster domain concentration ($[Ca^{2+}]_{dom}$), is a stationary quantity during sustained release periods and strongly depends on the type and amount of buffer. Particularly, it decreases drastically with higher concentrations of fast mobile buffer, but does not change with immobile buffer. There is therefore a clear correspondence of this relation to the relation of buffer with open probability (see Table 1). This also implies that buffers predominantly affect the open probability through tuning of interaction of channels, and not, as suggested by the single channel results, self-feedback. Our work thus supports the conjecture that fast mobile buffer (BAPTA) acts on communication between IP_3 Rs within a cluster (7).

Our results suggest that the spatial separation of channels within a cluster cannot be neglected. This finding contradicts earlier research, which concluded that all channels of a cluster can be subsumed in one source area. Swillens et al. (22) do not find differences in stochastic simulations of clusters when they considered spatial separation of 12 nm or channels homogeneously distributed in a virtual domain. The finding can be understood from the fact that domain calcium values for 12 nm should be larger than any dissociation constant and thus no difference in open probability to the virtual-domain approach appears. However, newer theoretical and experimental work suggests a much larger distance of channels and a cluster diameter of a few hundred nanometers (28,29). Our investigation indicates that in a large geometry domain, calcium concentrations are close to the dissociation constants of the subunit's binding sites. Therefore, the virtual domain cannot adequately describe the local calcium concentrations and its feedback on the channel gating.

We briefly compare the effects of buffer in our analysis to those found in experiments. A feature of the effect of BAPTA in our simulations is that with moderate amounts of BAPTA, inhibition of channels is reduced more strongly than activation. Because repeated spiking of calcium release is thought to incorporate inhibition of channels, we expect that for moderate amounts of BAPTA the decaying part of an oscillation, but not its activation, is eradicated. This behavior was indeed found in the experiments by Rintoul and Baimbridge (13). There it was shown that for cells without treatment, baseline spiking can be triggered. However, for moderate amounts of BAPTA, no spiking can be observed, while >40% of the cells respond with an active, monophasic state. In addition, we found that for large amounts of BAPTA, activation is also depressed. This finding provides an understanding of an important aspect in the experiments of Dargan et al. (14). The reduction of fluorescence peak level found there is reflected in our dependence of open fraction on BAPTA concentration (see Fig. 6).

We finally emphasize that, as suggested by Table 1, most of our results are consequences of the geometry of channel positioning, transport of Ca^{2+}, and the action of buffer rather than the single channel kinetic model. Our single cluster model thus captures essential processes during cell global calcium release independent of the concrete IP_3 R model. For instance, activation of channels by Ca^{2+} from neighboring open channels is a universal property of kinetic gating models with dissociation constant ~1 μM (30). Generally, for additional fast mobile buffer we then confirm the experimentally observed existence of a regime of reduced open probability (Fig. 5 *A* and Fig. 6). However, in our kinetic model, inhibition of channels requires the transition from the open to the closed state and is therefore dominated by domain calcium concentrations. This implies that intermediate concentrations of fast buffers can cause an increase of release amplitude by reduced inhibition (compare Fig. 5 *A*). In different models, as for instance the standard DeYoung-Keizer model (25), inhibition can occur in the open state of a channel, in which case the latter effect is not occurring and the up-arrow in P_o for fast buffer in Table 1 can disappear. Our analysis, in combination with experimental studies, may thus provide further cues for the verification of detailed and specific gating models.

SUPPORTING MATERIAL

Three additional sections with six equations, two tables, and four figures are available at http://www.biophysj.org/biophysj/supplemental/S0006-3495(10)00425-X.

This work was supported by grant No. FA 350/6-1 of the Deutsche Forschungsgemeinschaft within the priority program No. SPP 1095, "Analysis, Modeling, and Simulation of Multiscale Problems". J.W.S. acknowledges support from the National Science Foundation of China under grant No. 10775114 and National Institutes of Health grant No. 2R01GM065830-06A1.

REFERENCES

1. Berridge, M. J., M. D. Bootman, and H. L. Roderick. 2003. Calcium signaling: dynamics, homeostasis and remodeling. *Nat. Rev. Mol. Cell Biol.* 4:517–529.
2. Foskett, J. K., C. White, …, D. O. Mak. 2007. Inositol trisphosphate receptor Ca^{2+} release channels. *Physiol. Rev.* 87:593–658.

3. Parker, I., and Y. Yao. 1996. Ca^{2+} transients associated with openings of inositol trisphosphate-gated channels in *Xenopus* oocytes. *J. Physiol.* 491:663–668.
4. Marchant, J. S., and I. Parker. 2001. Role of elementary Ca^{2+} puffs in generating repetitive Ca^{2+} oscillations. *EMBO J.* 20:65–76.
5. Swillens, S., P. Champeil, …, G. Dupont. 1998. Stochastic simulation of a single inositol 1,4,5-trisphosphate-sensitive Ca^{2+} channel reveals repetitive openings during 'blip-like' Ca^{2+} transients. *Cell Calcium.* 23:291–302.
6. Shuai, J. W., and P. Jung. 2002. Stochastic properties of Ca^{2+} release of inositol 1,4,5-trisphosphate receptor clusters. *Biophys. J.* 83:87–97.
7. Dargan, S. L., and I. Parker. 2003. Buffer kinetics shape the spatiotemporal patterns of IP_3-evoked Ca^{2+} signals. *J. Physiol.* 553:775–788.
8. Zeller, S., S. Rüdiger, …, M. Falcke. 2009. Modeling of the modulation by buffers of Ca^{2+} release through clusters of IP_3 receptors. *Biophys. J.* 97:992–1002.
9. Rüdiger, S., and L. Schimansky-Geier. 2009. Dynamics of excitable elements with time-delayed coupling. *J. Theor. Biol.* 259:96–100.
10. Berridge, M. J. 1990. Calcium oscillations. *J. Biol. Chem.* 265: 9583–9586.
11. Rooney, T. A., E. J. Sass, and A. P. Thomas. 1989. Characterization of cytosolic calcium oscillations induced by phenylephrine and vasopressin in single Fura-2-loaded hepatocytes. *J. Biol. Chem.* 264:17131–17141.
12. Lechleiter, J., S. Girard, …, D. Clapham. 1991. Spiral calcium wave propagation and annihilation in *Xenopus laevis* oocytes. *Science.* 252:123–126.
13. Rintoul, G. L., and K. G. Baimbridge. 2003. Effects of calcium buffers and calbindin-D28k upon histamine-induced calcium oscillations and calcium waves in HeLa cells. *Cell Calcium.* 34:131–144.
14. Dargan, S. L., B. Schwaller, and I. Parker. 2004. Spatiotemporal patterning of IP3-mediated Ca^{2+} signals in *Xenopus* oocytes by Ca^{2+}-binding proteins. *J. Physiol.* 556:447–461.
15. Falcke, M. 2003. Buffers and oscillations in intracellular Ca^{2+} dynamics. *Biophys. J.* 84:28–41.
16. Wagner, J., and J. Keizer. 1994. Effects of rapid buffers on Ca^{2+} oscillations and Ca^{2+} diffusion. *Biophys. J.* 67:447–456.
17. Smith, G. D. 1996. Analytical steady-state solution to the rapid buffering approximation near an open Ca^{2+} channel. *Biophys. J.* 71:3064–3072.
18. Smith, G. D., J. Wagner, and J. Keizer. 1996. Validity of the rapid buffering approximation near a point source of calcium ions. *Biophys. J.* 70:2527–2539.
19. Smith, G., L. Dai, …, A. Sherman. 2001. Asymptotic analysis of buffered calcium diffusion near a point source. *SIAM J. Appl. Math.* 61:1816–1838.
20. Shuai, J., J. E. Pearson, and I. Parker. 2008. Modeling Ca^{2+} feedback on a single inositol 1,4,5-trisphosphate receptor and its modulation by Ca^{2+} buffers. *Biophys. J.* 95:3738–3752.
21. Shuai, J., J. E. Pearson, …, I. Parker. 2007. A kinetic model of single and clustered IP_3 receptors in the absence of Ca^{2+} feedback. *Biophys. J.* 93:1151–1162.
22. Swillens, S., G. Dupont, …, P. Champeil. 1999. From calcium blips to calcium puffs: theoretical analysis of the requirements for interchannel communication. *Proc. Natl. Acad. Sci. USA.* 96:13750–13755.
23. Shuai, J. W., and P. Jung. 2003. Optimal ion channel clustering for intracellular calcium signaling. *Proc. Natl. Acad. Sci. USA.* 100:506–510.
24. Shuai, J., D. Yang, …, S. Rüdiger. 2009. An investigation of models of the IPR channel in *Xenopus* oocyte. *Chaos.* 19:037105.
25. De Young, G. W., and J. Keizer. 1992. A single-pool inositol 1,4,5-trisphosphate-receptor-based model for agonist-stimulated oscillations in Ca^{2+} concentration. *Proc. Natl. Acad. Sci. USA.* 89:9895–9899.
26. Nagaiah, C., S. Rüdiger, …, M. Falcke. 2008. Adaptive numerical simulation of intracellular calcium dynamics using domain decomposition methods. *Appl. Numer. Math.* 58:1658.
27. Rüdiger, S., J. W. Shuai, …, M. Falcke. 2007. Hybrid stochastic and deterministic simulations of calcium blips. *Biophys. J.* 93:1847–1857.
28. Shuai, J., H. J. Rose, and I. Parker. 2006. The number and spatial distribution of IP_3 receptors underlying calcium puffs in *Xenopus* oocytes. *Biophys. J.* 91:4033–4044.
29. Demuro, A., and I. Parker. 2008. Multi-dimensional resolution of elementary Ca^{2+} signals by simultaneous multi-focal imaging. *Cell Calcium.* 43:367–374.
30. Sneyd, J., and M. Falcke. 2005. Models of the inositol trisphosphate receptor. *Prog. Biophys. Mol. Biol.* 89:207–245.